HHS Public Access

Author manuscript

*Angew Chem Int Ed Engl*. Author manuscript; available in PMC 2024 August 01.

Published in final edited form as:

*Angew Chem Int Ed Engl*. 2023 August 01; 62(31): e202219181. doi:10.1002/anie.202219181.

# Development of Dissolution Dynamic Nuclear Polarization of [$^{15}N_3$]Metronidazole: a Clinically Approved Antibiotic

**David O. Guarin**[a,b], **Sameer M. Joshi**[c], **Anna Samoilenko**[c], **Mohammad S. H. Kabir**[c], **Erin E. Hardy**[a], **Atsushi M. Takahashi**[d], **Jan H. Ardenkjaer-Larsen**[b,e], **Eduard Y. Chekmenev**[c,f], **Yi-Fen Yen**[a]

[a]Department of Radiology, Athinoula A. Martinos Center for Biomedical Imaging, Massachusetts General Hospital, 149 13th St., Charlestown, Massachusetts, 02129, United States

[b]Polarize ApS., Asmussens Alle 1, Frederiksberg, 1808 Denmak

[c]Department of Chemistry, Integrative Biosciences (Ibio), Karmanos Cancer Institute (KCI), Wayne State University, Detroit, Michigan 48202, United States

[d]Department of Brain and Cognitive Sciences, McGovern Institute for Brain Research, Massachusetts Institute of Technology, Cambridge, Massachusetts, 02139, United States

[e]Department of Health Technology, Technical University of Denmark, 348, Ørsteds Pl., Kongens Lyngby, 2800, Denmark

[f]Russian Academy of Sciences (RAS), 14 Leninskiy Prospekt, 119991 Moscow, Russia

## Abstract

We report dissolution Dynamic Nuclear Polarization (d-DNP) of [$^{15}N_3$]metronidazole ([$^{15}N_3$]MNZ) for the first time. Metronidazole is a clinically approved antibiotic, which can be potentially employed as a hypoxia-sensing molecular probe using $^{15}N$ hyperpolarized (HP) nucleus. DNP process is very efficient for [$^{15}N_3$]MNZ with an exponential build-up constant of 13.8 min using trityl radical. After dissolution and sample transfer to a nearby 4.7 T Magnetic Resonance Imaging scanner, HP [$^{15}N_3$]MNZ lasted remarkably long with $T_1$ values up to 343 s and $^{15}N$ polarizations up to 6.4%. A time series of HP [$^{15}N_3$]MNZ images was acquired *in-vitro* using a steady state free precession sequence on the $^{15}NO_2$ peak. The signal lasted over 13 min with notably long $T_2$ of 20.5 s. HP [$^{15}N_3$]MNZ was injected in the tail vein of a healthy rat, and

Dr. D. O. Guarin, Department of Radiology, Athinoula A. Martinos Center for Biomedical Imaging, Massachusetts General Hospital, 149 13th St., Charlestown, Massachusetts, 02129, United States, dguarinbedoya@mgh.harvard.edu, Dr. Y. Yen, Department of Radiology, Athinoula A. Martinos Center for Biomedical Imaging, Massachusetts General Hospital, 149 13th St., Charlestown, Massachusetts, 02129, United States, yyen1@mgh.harvard.edu.

Supporting information for this article is given via a link at the end of the document.

Conflict of Interest
E.Y.C. has a stake of ownership in XeUS Technologies LTD.
J.H.A-L is the owner of Polarize ApS.

Twiter Handles:
@MGHMartinos
@davidoguarinb
@e_chekmenev
@waynestatechem

dynamic spectroscopy was performed over the rat brain. The *in-vivo* HP $^{15}N$ signals persisted over 70 s, demonstrating an unprecedented opportunity for *in-vivo* studies.

## Graphical Abstract

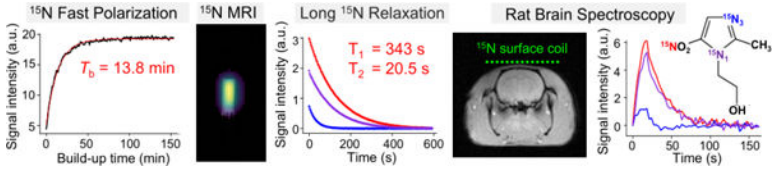


[$^{15}N_3$]Metronidazole (MNZ) is an emerging hyperpolarized contrast agent. The Dynamic Nuclear Polarization process of this clinically used antibiotic is very fast compared to many other $^{15}N$-labeled molecules and has remarkably long $T_1$ and $T_2$. The hyperpolarized signal of MNZ lasted for over a minute in a rat brain. Future work on hyperpolarized MNZ will investigate its potential as an antibiotic or hypoxia-sensing probe in disease models.

### Keywords

dissolution-DNP; hyperpolarization; NMR spectroscopy; nitrogen-15; imaging agents

## Introduction:

Hyperpolarization of nuclear spins increases nuclear spin polarization up to 5 orders of magnitude. Hyperpolarized (HP) molecules employed as exogenous magnetic resonance (MR) contrast agents are non-radioactive and can be used to non-invasively study *in-vivo* biophysiology, such as metabolism,[1–15] perfusion,[6–9] or pH[10–12] in real time. In recent years, promising *in-vivo* HP imaging applications have led to increasing interest in the search for new HP molecular probes for magnetic resonance imaging (MRI)[1,6,13,14] and magnetic resonance spectroscopy (MRS).[6,15–17] Among the multiple hyperpolarization techniques[18–22] developed to date, parahydrogen-based hyperpolarization processes, such as Signal Amplification by Reversible Exchange (SABRE)[20–23], and dissolution dynamic nuclear polarization (d-DNP)[24–28] have demonstrated excellent signal enhancements of many metabolites and biocompatible molecules supporting a wide range of studies in biological systems, most notably in cancer[14–29].

The development of HP contrast agents relies mainly on the use of isotopically labeled compounds, where the type of isotope labels (e.g., $^{13}C$, $^{15}N$) and site of labeling in the molecular structure are specifically chosen for the desired application[28]. In MR experiments, the use of nuclei with low gyromagnetic ratios, such as $^{13}C$ or $^{15}N$, benefits from wide chemical-shift dispersion of spectral resonances, making it easy to distinguish peaks of different metabolites and quantify results. Moreover, unlike protons, $^{13}C$ and $^{15}N$ nuclei have virtually no background signal. In addition, $^{13}C$ and $^{15}N$ labeled molecules often possess long longitudinal relaxation times ($T_1$), which allows them to retain HP state for a long time, therefore, making these nuclei great candidates for utility in HP MRI contrast agents[5,14,30–34]. However, the characteristically low MR $^{15}N$ sensitivity, ~1/6 of the $^{13}C$

MR sensitivity, limits $^{15}N$ *in-vivo* applications[16]. $^{13}C$ labeled compounds have, therefore, been the primary focus on the development of HP contrast agents. To date, many HP $^{13}C$-labeled molecules have been developed [11,35–37] and demonstrated utility in a wide range of *in-vivo* imaging applications in animal and clinical research.[3,10,11,36] [1-$^{13}C$]pyruvate in particular has been the key molecule for *in-vivo* HP $^{13}C$ MR studies because of its central role in cellular energy metabolism[3,4,38] and also importantly, its long $^{13}C$ carboxyl $T_1$ (~68 s in solution and ~ 30 s *in-vivo* at 3 T).

Despite the low MR sensitivity, some $^{15}N$ compounds have the merit of very long $T_1$ relaxation times in specific $^{15}N$ sites, reaching up to 20 min $T_1$.[39–41] Despite the substantial potential of $^{15}N$ HP molecular probes for *in-vivo* applications[16], there have been less than a handful of demonstrated *in-vivo* applications[16] including choline, [42] urea[34] and carnitine.[43] Choline and carnitine are tertiary amines with symmetric structures rendering high symmetry of $^{15}N$ site and resulting in long $T_1$. The nitro- moieties present in compounds that are used as, antibiotics,[44] hypoxia sensors[45, or cancer radio-sensitizing agents[46] are also characterized by long $T_1$ reaching up to 20 min in liquid state.[47]

There is a large family of antibiotics called the nitroimidazoles known for their actions on several anaerobic bacterial infections.[44,48] Furthermore, nitroimidazoles can bind to different cellular macromolecules, particularly in hypoxic conditions, allowing them to be used as exogenous hypoxia markers.[45,46,48] In cancer, most tumors are characterized by a hypoxic micro-environment in which the oxygen concentrations and pH are lower than for normal tissue. The hypoxic status has been demonstrated in various tumors to be an indicator of unfavorable prognosis, which is related to cancer progression with an increased probability of metastasis.[45,48] Nitroimidazoles' ability to probe hypoxic conditions has therefore been utilized for cancer screening using positron emission tomography (PET)[48] and both MRS and MRI.[45,46] HP nitro- moieties have not been demonstrated *in-vivo* prior to this report, although several nitroimidazoles have been HP by a method called SABRE in SHield Enables Alignment Transfer to Heteronuclei (SABRE-SHEATH)[50–52].

Metronidazole (MNZ) is a member of the nitroimidazoles group and is also an antibiotic approved by the United States Food and Drug Administration (FDA) to treat a wide variety of infections. Large dosage is allowed for intravenous injection – a single dose of MNZ injection (known as Flagyl Injection) containing 500 mg metronidazole[53]. In addition, MNZ's $^{15}N$ sites have shown to have long $T_1$ relaxation times (several minutes), [47]. Such a long $T_1$ greatly complements the biological compatibility of this contrast agent. Furthermore, the hypoxia sensing potential and antibiotic functionality of MNZ makes it a very interesting candidate to be used as a HP contrast agent to probe hypoxia, to test drug delivery or to perform cancer screening. Previously, we have reported HP [$^{15}N_3$]metronidazole ([$^{15}N_3$]MNZ) using SABRE technique.[47,52] Although the SABRE technique presents multiple advantages for hyperpolarizing $^{15}N$-labeled compounds, it has not been translated *in-vivo* yet. However, biocompatible formulations have recently been demonstrated for [1-$^{13}C$]pyruvate[54] and therefore, could be potentially extended to HP [$^{15}N_3$]metronidazole in the near future.

In this work, we employed d-DNP technique to hyperpolarize [$^{15}N_3$]MNZ to obtain a biocompatible solution for *in-vivo* experiments. Using a state-of-the-art d-DNP polarizer (SpinAliner®, Polarize, ApS, Denmark)[54] that was tuned to $^{15}N$ frequency, we were able to monitor the polarization buildup which aided in the optimization of the [$^{15}N_3$]MNZ sample formulation (Figure 1). Here we report our methods to hyperpolarize [$^{15}N_3$]MNZ in a biocompatible formulation, the liquid state polarization, $T_1$ and $T_2$ relaxation times of the injectable solution, and the feasibility for *in-vivo* [$^{15}N_3$]MNZ MRS in a rat.

## Results and Discussion

The DNP sample of [$^{15}N_3$]MNZ was optimized in several steps. A maximum MNZ concentration of 1.5 M was achieved by dissolving MNZ in >99.7% dimethyl sulfoxide (DMSO), which also avoided otherwise undesirable crystallization of the sample at cryogenic temperatures. Moreover, trityl (AH111501) is very soluble in DMSO, which resulted in a homogeneous radical distribution (with 30 mM AH111501). Although other sample mixtures containing water, glycerol, and DMSO were tested, no other solution could achieve a MNZ concentration above 1 M. For example, in a mixture of 1:1 glycerol:water, the maximum achievable MNZ concentration was only ~ 0.25 M, which would have been diluted to ~ 12 mM after dissolution and exceedingly challenging to detect in animal studies. The concentration of 1.5 M achievable in DMSO yielded ~ 75 mM concentration after dissolution, which is comparable to the concentration of hyperpolarized $^{13}C$-labeled substrates used in animal research today[26,55]. Regarding the biocompatibility of DMSO, the 21-fold dilution (**see** Supporting Information or SI) occurred during the dissolution process reduced the concentration of DMSO to a level that is comparable to the concentration used in several therapeutical treatments for interstitial cystitis[56] and amyloidosis[57,58], among other diseases[59]. Therefore, the DMSO toxicity is not a concern.

The $^{15}N$ polarization build-up performed at an optimal microwave frequency (**see** SI) revealed the unusually fast mono-exponential build-up time constant ($T_b$) of 13.8 ± 0.2 min (**see** SI). Previously reported build-up rates for long-$T_1$ $^{15}N$ sites have been shown substantially greater: *e.g.*, $^{15}N$ choline $T_b$=45±3 mins.[42] This result is important because short $T_b$ values allow for full polarization build-up substantially faster—for example, near steady-state $^{15}N$ polarization was achieved in less than one hour for [$^{15}N_3$]MNZ. In comparison, typical $^{15}N$ DNP experiments are performed for several hours because of the high $T_b$ values.[43]

An example of the first $^{15}N$ spectrum of a dynamic spectroscopy experiment is displayed in Figure 2a. The signal of the three $^{15}N$ sites can be observed in the first scan with enhancements of ~ 20560, ~30647, and ~ 7144 for $^{15}N_1$, $^{15}NO_2$, and $^{15}N_3$, respectively. The thermal equilibrium spectrum is also displayed in Figure 2c. The $^{15}N$ $T_1$ relaxation times for $^{15}N_1$ and $^{15}NO_2$ at 4.7 T were long, 262±2 s and 343±3 s, respectively. The $T_1$ of $^{15}N_3$ was 41.2±0.2 s, which is substantially shorter than that of the other two $^{15}N$ sites, yet it is still comparable to that of many $^{13}C$-labeled HP contrast agents. The vast difference in the $^{15}N$ $T_1$ values may be due to different electronic properties of the sites (and thus, by the Chemical Shift Anisotropy relaxation contribution), and the fact that this $^{15}N$ site participates in the proton exchange, and thus, maybe more susceptible to other

solute-induced sources of $T_1$ relaxation. Based on the measured enhancement levels (Figure 2b), the polarization at the time of dissolution was determined to be 5.2%, 6.4%, and 4.6 % for $^{15}N_1$, $^{15}NO_2$, and $^{15}N_3$, respectively.

A modified balanced steady state free precession (bSSFP) sequence was used to acquire a series of 1000 images of a syringe containing HP [$^{15}N_3$]MNZ (Figure 3). The sequence was modified so that an α/2 pulse was applied prior to the first repetition only, and so that no additional α/2 pulses were applied between subsequent averages or repetitions. Moreover, frequency-selective RF excitation pulses were employed to selectively image HP $^{15}NO_2$ resonance. $^{15}NO_2$ HP images were obtained with a max signal-to-noise ratio (SNR) of 67 in the first image of the bSSFP experiment (Figure 3d). The SNR obtained by averaging the first 200 images is 305.

The bSSFP signal was used to model the $T_2$ of $^{15}NO_2$ (Figure 3d) using the equation developed by Scheffler[60,61], adapted for HP imaging.[62,63] The $^{15}NO_2$ $T_2$ relaxation time at 4.7 T was long, 20.5±0.4 s. To confirm the $T_2$ measurement, a bSSFP experiment was done with a HP [1-$^{13}$C]acetate phantom (**see** SI). The determined $^{13}C$ $T_2$ of HP [1-$^{13}$C]acetate was 4.6 s, which is similar to the previously reported value.[1–15][17] The long-lasting HP [$^{15}N_3$]MNZ imaging signal in the bSSFP acquisition was remarkable, which is rationalized by the correspondingly long $T_1$ and $T_2$ values.[17,63] The long-lasting HP signal indicates a good potential for *in-vivo* $^{15}N$ imaging applications.

Results of the pilot *in-vivo* study using tail-vein bolus injection of HP [$^{15}N_3$]MNZ are displayed in Figure 4. Note that the spatial localization in this experiment is achieved using a surface coil placed over the rat head. Since the blood flow to the brain is vastly greater than that to the rest of the head tissues, we attribute the detected $^{15}N$ signals to those in cerebral vasculature and brain tissues. The *in-vivo* dynamic MRS acquisition started approximately 5 seconds after the start of injection. The signal time curves (Figure 4d) showed that [$^{15}N_3$]MNZ reached the brain within 5 seconds after the start of injection and the signal reached maximum in 15–20 seconds. The HP signal lasted for over a minute after injection providing an excellent time window for neuroimaging applications. The highest SNR values are obtained by adding scans 3–9, ~227, ~270, and ~60 for $^{15}N_1$, $^{15}NO_2$, and $^{15}N_3$, respectively (spectrum displayed in Figure 4a). SNR values are ~ 57, ~66, and ~ 13 for $^{15}N_1$, $^{15}NO_2$, and $^{15}N_3$, respectively, for scan 7. The SNR of the pilot experiment can be substantially improved through the use of singular value decomposition to suppress the noise[64].

The dynamics of *in-vivo* $^{15}N$ MRS with respect to the injection duration and the arrival of the MNZ bolus are depicted in Figure 4d. The reader should be reminded that the signal rise is attributed to the arrival of the HP [$^{15}N_3$]MNZ bolus to the brain, and the signal decay is associated with both the bolus washout from the brain and the $^{15}N$ $T_1$ relaxation. The apparent $^{15}N$ signal decay time constant (Tm) during the HP [$^{15}N_3$]MNZ bolus washout was estimated by fitting to a mono-exponential decay of the signal time curves (region to the right of the black dotted line in Figure 4d): 24.3 ± 0.4 s and 24.7 ± 0.7 for $^{15}N_1$ and $^{15}NO_2$ sites, respectively (the respective time constant for $^{15}N_3$ site was challenging to determine due to low SNR).

To understand the fast signal decays observed from the rat head, we measured the $T_1$ decay time constants of the three $^{15}N$ labels of [$^{15}N_3$]MNZ in blood serum and in $D_2O$ (as a reference solution) at 1.4 T (SpinSolve 60 MHz benchtop spectrometer by Magritek, Wellington, New Zealand) under the same experimental conditions (**see** SI). The resulting $^{15}N$ $T_1$ for $^{15}N_1$, $^{15}NO_2$, and $^{15}N_3$ sites in serum were 47 ± 2 s, 81 ± 3 s, and 36 ± 2 s, respectively, compared to 119 ± 4 s, 212 ± 6 s, and 20 ± 5 s in $D_2O$. The $T_1$ values in serum were smaller than those in $D_2O$, as expected. The $T_1$ values in serum were much larger than the apparent $^{15}N$ signal decay time constants (Tm) measured in the rat head for both the $^{15}N_1$ and $^{15}NO_2$ sites (Figure 4b). Furthermore, the $T_1$ value of the $^{15}NO_2$ site in serum (81 ± 3 s) was significantly larger than the $T_1$ of the $^{15}N_1$ site (47 ± 2 s) and yet the Tm values in the rat head were both reduced to very comparable values (24.3 ± 0.4 s and 24.7 ± 0.7 s for $^{15}N_1$ and $^{15}NO_2$, respectively). These observations suggested that the signals of $^{15}N_1$ and $^{15}NO_2$ *in vivo* were both affected by a common and strong mechanism responsible for the fast signal decay *in vivo*. This mechanism *in vivo* is likely to be washout from the bloodstream in the brain.

Specifically, we envision that this FDA-approved antibiotic could be employed as hypoxia sensing molecular probe. As the first step towards this goal, we performed computational studies to determine the $^{15}N$ chemical shifts of putative metabolites of downstream [$^{15}N_3$]MNZ metabolism in a hypoxic environment. The calculated $^{15}N$ chemical shifts (157 ppm, 249 ppm, and 343 ppm for $^{15}N_1$, $^{15}N_3$ and $^{15}NO_2$, respectively) match remarkably well to the measured chemical shifts (166 ppm, 249 ppm, and 357 ppm, respectively) of the three $^{15}N$ in [$^{15}N_3$]metronidazole (Figure 5). These simulation results gave us confidence for the predicted large $^{15}N$ chemical shifts of the reduced [$^{15}N_3$]metronidazole (Figure 5), which should be well differentiated from the injected [$^{15}N_3$]metronidazole in hypoxic conditions. The stepwise reduction of the $^{15}NO_2$ moiety results in substantial changes (of up to 390 ppm) of all $^{15}N$ sites, *i.e.*, all three $^{15}N$ sites can sense the reduction of nitro group through the changes in their chemical shifts. This represents a clear translational advantage of employing a multi-chromatic HP probe. However, the reader should be reminded that the directly attached protons in the downstream metabolites would likely render short $^{15}NO_2$ $T_1$ in hydroxylamino- and amino-derivatives making them likely undetectable – this is not a fundamental limitation of this potential metabolic sensor as $^{15}N_1$ and $^{15}N_2$ sites will likely not experience any $T_1$ changes through these chemical transformations, and they have sufficient chemical shift dispersion for spectroscopic sensing of putative metabolites. No metabolites were detected via $^{15}N$ MRS in this pilot study because we employed healthy rat without any brain hypoxia or infection. All in all, the presented pilot results here represent a substantial advance over the previous report to isotopically enrich [$^{15}N_3$]metronidazole and perform mechanistic SABRE studies. While $^{15}N$ polarization in the SABRE studies was higher ($P_{15N}$ ~ 16%) than the one reported here (~6%), it should be noted that the product of polarization and the concentration (*i.e.*, polarization payload) is nearly the same in this study employing d-DNP versus previous SABRE studies. However, most importantly the d-DNP prepared $^{15}N$ polarization payload is already biologically compatible, which we demonstrated here, whereas SABRE technology has not been translated *in vivo* with any contrast agent (*ca.* 12/2022), to the best of our knowledge. We have also reported the computational studies of $^{15}N$ chemical shifts that can act as the potential reporters to sense

hypoxia *in vivo*. The pilot results reported here indeed bode well for future systematic *in-vivo* studies. Specifically, we envision the applications related to hypoxia sensing in stroke, brain trauma, neurodegenerative diseases, resistance to radiotherapy in solid cancer tumors, and others.

## Conclusion:

In this study, we utilized d-DNP for efficient $^{15}N$ hyperpolarization of uniformly $^{15}N$-labeled metronidazole. The DNP sample formulation that we developed resulted in an exceptionally fast $^{15}N$ polarization build-up constant of 13.8 ± 0.2 mins. $^{15}N$ polarization of over 6% was obtained after approximately a 30-second-long process to transfer the sample from the polarizer to the MRI scanner. Dissolution yielded ~ 75 mM HP [$^{15}N_3$]MNZ in aqueous biocompatible media suitable for *in-vivo* applications. Very long $^{15}N$ $T_1$, exceeding 5 minutes in solution after dissolution, was observed for the $^{15}NO_2$ site at 4.7 T. We have successfully demonstrated the feasibility of *in-vitro* $^{15}N$ MRI using bSSFP imaging sequence and obtained remarkably long-lasting bSSFP signal on $^{15}NO_2$ due to its very long $T_2$. Finally, we have also performed a pilot *in-vivo* demonstration using tail-vein intravenous injection of HP [$^{15}N_3$]MNZ in a healthy rat. HP $^{15}N$ signals were successfully detected over 1 minute after the bolus of HP [$^{15}N_3$]MNZ was delivered to the brain. Fast DNP $^{15}N$ polarization buildup, good levels of $^{15}N$ polarization, and exceedingly long $^{15}N$ $T_1$ and $T_2$ of HP [$^{15}N_3$]MNZ bode well for HP MRI experiments in general, which will be developed in future studies to explore potential biomedical applications of this FDA-approved antibiotic as an antibiotic or hypoxia probe.

## Supplementary Material

Refer to Web version on PubMed Central for supplementary material.

## Acknowledgments

This work was supported by NIH funds S10OD021768, R21GM137227, R01EB029829, NSF CHE-1904780. The content is solely the responsibility of the authors and does not necessarily represent the official views of the National Institutes of Health. We thank Dr. Jonathan R. Birchall for pilot solubility testing of metronidazole in DMSO.

## References:

[1]. Golman K, Petersson JS, Acad Radiol 2006, 13, 932–942. [PubMed: 16843845]

[2]. Hurd RE, Yen Y, Chen A, Ardenkjaer-Larsen JH, J Magn Reson Imaging 2012, 36, 1314–1328. [PubMed: 23165733]

[3]. Kohler SJ, Yen Y, Wolber J, Chen AP, Albers MJ, Bok R, Zhang V, Tropp J, Nelson S, Vigneron DB, Kurhanewicz J, Hurd RE, Magn Reson Med 2007, 58, 65–69. [PubMed: 17659629]

[4]. Nelson SJ, Kurhanewicz J, Vigneron DB, Larson PEZ, Harzstark AL, Ferrone M, van Criekinge M, Chang JW, Bok R, Park I, Reed G, Carvajal L, Small EJ, Munster P, Weinberg VK, Ardenkjaer-Larsen JH, Chen AP, Hurd RE, Odegardstuen L-I, Robb FJ, Tropp J, Murray JA, Sci Transl Med 2013, 5, DOI 10.1126/scitranslmed.3006070.

[5]. Park I, Larson PEZ, Zierhut ML, Hu S, Bok R, Ozawa T, Kurhanewicz J, Vigneron DB, VandenBerg SR, James CD, Nelson SJ, Neuro Oncol 2010, 12, 133–144. [PubMed: 20150380]

[6]. Schroeder MA, Clarke K, Neubauer S, Tyler DJ, Circulation 2011, 124, 1580–1594. [PubMed: 21969318]

[7]. Johansson E, Månsson S, Wirestam R, Svensson J, Petersson JS, Golman K, Ståhlberg F, Magn Reson Med 2004, 51, 464–472. [PubMed: 15004786]

[8]. Johansson E, Olsson LE, Månsson S, Petersson JS, Golman K, Ståhlberg F, Wirestam R, Magn Reson Med 2004, 52, 1043–1051. [PubMed: 15508152]

[9]. von Morze C, Bok RA, Reed GD, Ardenkjaer-Larsen JH, Kurhanewicz J, Vigneron DB, Magn Reson Med 2014, 72, 1599–1609. [PubMed: 24382698]

[10]. Düwel S, Hundshammer C, Gersch M, Feuerecker B, Steiger K, Buck A, Walch A, Haase A, Glaser SJ, Schwaiger M, Schilling F, Nat Commun 2017, 8, 15126. [PubMed: 28492229]

[11]. Gallagher FA, Kettunen MI, Day SE, Hu D-E, Ardenkjær-Larsen JH, in ‘t Zandt R, Jensen PR, Karlsson M, Golman K, Lerche MH, Brindle KM, Nature 2008, 453, 940–943. [PubMed: 18509335]

[12]. Gallagher FA, Kettunen MI, Brindle KM, NMR Biomed 2011, 24, 1006–1015. [PubMed: 21812047]

[13]. Golman K, Olsson LE, Axelsson O, Månsson S, Karlsson M, Petersson JS, Br J Radiol 2003, 76, S118–S127. [PubMed: 15572334]

[14]. Kurhanewicz J, Vigneron DB, Ardenkjaer-Larsen JH, Bankson JA, Brindle K, Cunningham CH, Gallagher FA, Keshari KR, Kjaer A, Laustsen C, Mankoff DA, Merritt ME, Nelson SJ, Pauly JM, Lee P, Ronen S, Tyler DJ, Rajan SS, Spielman DM, Wald L, Zhang X, Malloy CR, Rizi R, Neoplasia 2019, 21, 1–16. [PubMed: 30472500]

[15]. Goodson BM, Whiting N, Coffey AM, Nikolaou P, Shi F, Gust BM, Gemeinhardt ME, Shchepin R. v., Skinner JG, Birchall JR, Barlow MJ, Chekmenev EY, in EMagRes, John Wiley & Sons, Ltd, Chichester, UK, 2015, pp. 797–810.

[16]. Park H, Wang Q, Chem Sci 2022, 13, 7378–7391. [PubMed: 35872812]

[17]. Varma G, Wang X, Vinogradov E, Bhatt RS, Sukhatme VP, Seth P, Lenkinski RE, Alsop DC, Grant AK, Magn Reson Med 2016, 76, 1102–1115. [PubMed: 26507361]

[18]. Abragam A, Proctor WG, Phys Rev 1958, 109, 1441–1458.

[19]. Abragam A, Goldman M, Rep Prog Phys 1978, 41, 395–467.

[20]. Adams RW, Aguilar JA, Atkinson KD, Cowley MJ, Elliott PIP, Duckett SB, Green GGR, Khazal IG, López-Serrano J, Williamson DC, Science (1979) 2009, 323, 1708–1711.

[21]. Goodson BM, J Magn Reson 2002, 155, 157–216. [PubMed: 12036331]

[22]. Bowers CR, Weitekamp DP, Phys Rev Lett 1986, 57, 2645–2648. [PubMed: 10033824]

[23]. Mewis RE, Magn Reson Chem 2015, 53, 789–800. [PubMed: 26264565]

[24]. Ardenkjaer-Larsen JH, J Magn Reson 2016, 264, 3–12. [PubMed: 26920825]

[25]. Jähnig F, Kwiatkowski G, Ernst M, J Magn Reson 2016, 264, 22–29. [PubMed: 26920827]

[26]. Comment A, J Magn Reson 2016, 264, 39–48. [PubMed: 26920829]

[27]. Ardenkjær-Larsen JH, Fridlund B, Gram A, Hansson G, Hansson L, Lerche MH, Servin R, Thaning M, Golman K, Proc Nattll Acad Sci USA 2003, 100, 10158–10163.

[28]. Jannin S, Dumez J-N, Giraudeau P, Kurzbach D, J Magn Reson 2019, 305, 41–50. [PubMed: 31203098]

[29]. Kurhanewicz J, Vigneron DB, Brindle K, Chekmenev EY, Comment A, Cunningham CH, DeBerardinis RJ, Green GG, Leach MO, Rajan SS, Rizi RR, Ross BD, Warren WS, Malloy CR, Neoplasia 2011, 13, 81–97. [PubMed: 21403835]

[30]. Gabellieri C, Reynolds S, Lavie A, Payne GS, Leach MO, Eykyn TR, J Am Chem Soc 2008, 130, 4598–4599. [PubMed: 18345678]

[31]. Fekete M, Ahwal F, Duckett SB, J Phys Chem B 2020, 124, 4573–4580. [PubMed: 32383603]

[32]. Olaru AM, Burns MJ, Green GGR, Duckett SB, Chem Sci 2017, 8, 2257–2266. [PubMed: 28507682]

[33]. Iali W, Roy SS, Tickner BJ, Ahwal F, Kennerley AJ, Duckett SB, Angew Chem 2019, 131, 10377–10381.

[34]. Durst M, Chiavazza E, Haase A, Aime S, Schwaiger M, Schulte RF, Magn Reson Med 2016, 76, 1900–1904. [PubMed: 26822562]

[35]. Cabella C, Karlsson M, Canapè C, Catanzaro G, Colombo Serra S, Miragoli L, Poggi L, Uggeri F, Venturi L, Jensen PR, Lerche MH, Tedoldi F, J Magn Reson 2013, 232, 45–52. [PubMed: 23689113]

[36]. Keshari KR, Wilson DM, Chen AP, Bok R, Larson PEZ, Hu S, van Criekinge M, Macdonald JM, Vigneron DB, Kurhanewicz J, J Am Chem Soc 2009, 131, 17591–17596. [PubMed: 19860409]

[37]. von Morze C, Larson PEZ, Hu S, Keshari K, Wilson DM, Ardenkjaer-Larsen JH, Goga A, Bok R, Kurhanewicz J, Vigneron DB, J Magn Reson Imaging 2011, 33, 692–697. [PubMed: 21563254]

[38]. Serrao EM, Brindle KM, Front Oncol 2016, 6, DOI 10.3389/fonc.2016.00059.

[39]. Shchepin R. v., Jaigirdar L, Chekmenev EY, J Phys Chem C 2018, 122, 4984–4996.

[40]. Nonaka H, Hirano M, Imakura Y, Takakusagi Y, Ichikawa K, Sando S, Sci Rep 2017, 7, 40104. [PubMed: 28067292]

[41]. Theis T, Ortiz GX, Logan AWJ, Claytor KE, Feng Y, Huhn WP, Blum V, Malcolmson SJ, Chekmenev EY, Wang Q, Warren WS, Sci Adv 2016, 2, DOI 10.1126/sciadv.1501438.

[42]. Cudalbu C, Comment A, Kurdzesau F, van Heeswijk RB, Uffmann K, Jannin S, Denisov V, Kirik D, Gruetter R, Phys Chem Chem Phys 2010, 12, 5818. [PubMed: 20461252]

[43]. Morze C, Engelbach JA, Reed GD, Chen AP, Quirk JD, Blazey T, Mahar R, Malloy CR, Garbow JR, Merritt ME, Magn Reson Med 2021, 85, 1814–1820. [PubMed: 33179825]

[44]. Upcroft P, Upcroft JA, Clin Microbiol Rev 2001, 14, 150–164. [PubMed: 11148007]

[45]. Kizaka-Kondoh S, Konse-Nagasawa H, Cancer Sci 2009, 100, 1366–1373. [PubMed: 19459851]

[46]. Bonnet M, Hong CR, Wong WW, Liew LP, Shome A, Wang J, Gu Y, Stevenson RJ, Qi W, Anderson RF, Pruijn FB, Wilson WR, Jamieson SMF, Hicks KO, Hay MP, J Med Chem 2018, 61, 1241–1254. [PubMed: 29253343]

[47]. Shchepin R. v., Birchall JR, Chukanov N. v., Kovtunov K. v., Koptyug I. v., Theis T, Warren WS, Gelovani JG, Goodson BM, Shokouhi S, Rosen MS, Yen Y, Pham W, Chekmenev EY, Chem Eur J 2019, 25, 8829–8836. [PubMed: 30964568]

[48]. Masaki Y, Shimizu Y, Yoshioka T, Tanaka Y, Nishijima K, Zhao S, Higashino K, Sakamoto S, Numata Y, Yamaguchi Y, Tamaki N, Kuge Y, Sci Rep 2015, 5, 16802. [PubMed: 26582591]

[49]. Feng X, Li Y, Zhang S, Li C, Tian J, J Nanobiotechnology 2022, 20, 142. [PubMed: 35303862]

[50]. Salnikov OG, Chukanov N. v., Svyatova A, Trofimov IA, Kabir MSH, Gelovani JG, Kovtunov K. v., Koptyug I. v., Chekmenev EY, Angew Chem Int Ed 2021, 60, 2406–2413.

[51]. Birchall JR, Kabir MSH, Salnikov OG, Chukanov N. v., Svyatova A, Kovtunov K. v., Koptyug I. v., Gelovani JG, Goodson BM, Pham W, Chekmenev EY, ChemComm 2020, 56, 9098–9101.

[52]. Barskiy DA, Shchepin RV, Coffey AM, Theis T, Warren WS, Goodson BM, Chekmenev EY, J Am Chem Soc 2016, 138, 8080–8083. [PubMed: 27321159]

[53]. Food and Drug Administration of the United States, “METRONIDAZOLE Injection, USP,” can be found under https://www.accessdata.fda.gov/drugsatfda_docs/label/2018/018890s052lbl.pdf., 2018.

[54]. Schmidt AB, de Maissin H, Adelabu I, Nantogma S, Ettedgui J, TomHon P, Goodson BM, Theis T, Chekmenev EY, ACS Sens 2022, 7, 3430–3439. [PubMed: 36379005]

[55]. Yen Y-F, Le Roux P, Mayer D, King R, Spielman D, Tropp J, Butts Pauly K, Pfefferbaum A, Vasanawala S, Hurd R, NMR Biomed 2010, n/a-n/a.

[56]. Parkin J, Shea C, Sant GR, J Urol 1998, 159, 2253–2253.

[57]. Burgess JL, Hamner AP, Robertson WO, Vet Hum Toxicol 1998, 40, 87–9. [PubMed: 9554060]

[58]. McCammon KA, Lentzner AN, Moriarty RP, Schellhammer PF, Urology 1998, 52, 1136–1138. [PubMed: 9836571]

[59]. Santos NC, Figueira-Coelho J, Martins-Silva J, Saldanha C, Biochem Pharmacol 2003, 65, 1035–1041. [PubMed: 12663039]

[60]. Scheffler K, Magn Reson Med 2003, 49, 781–783. [PubMed: 12652552]

[61]. Scheffler K, Lehnhardt S, Eur Radiol 2003, 13, 2409–2418. [PubMed: 12928954]

[62]. Svensson J, Månsson S, Johansson E, Petersson JS, Olsson LE, Magn Reson Med 2003, 50, 256–262. [PubMed: 12876701]

[63]. Milshteyn E, Reed GD, Gordon JW, von Morze C, Cao P, Tang S, Leynes AP, Larson PEZ, Vigneron DB, J Magn Reson 2020, 312, 106691. [PubMed: 32058912]

[64]. Coffey AM, Feldman MA, Shchepin R. v., Barskiy DA, Truong ML, Pham W, Chekmenev EY, J Magn Reson 2017, 281, 246–252. [PubMed: 28651245]

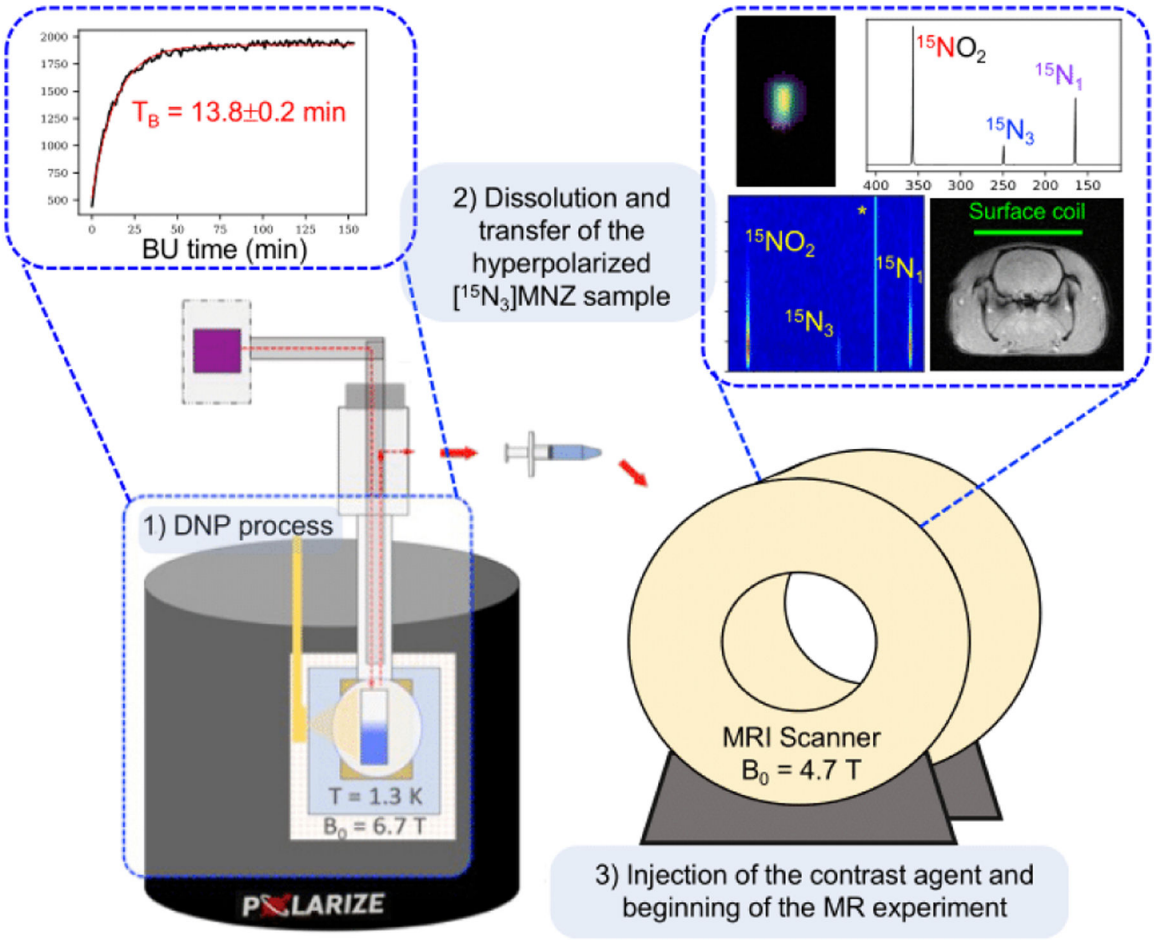


**Figure 1.**

Schematic of a d-DNP experiment. The [$^{15}N_3$]metronidazole ([$^{15}N_3$]MNZ) samples were HP (1) at cryogenic temperature and under microwave irradiation in a d-DNP polarizer, where the build-up (BU) of the polarization was monitored. After reaching maximum polarization, the sample was dissolved (2) with a warm solvent and collected into a syringe. The syringe was rapidly transferred to an MRI scanner where the MRS or MRI experiment was performed (3). (*) [$^{15}N_2$]imidazole resonance of a phantom positioned on the top of the surface coil.

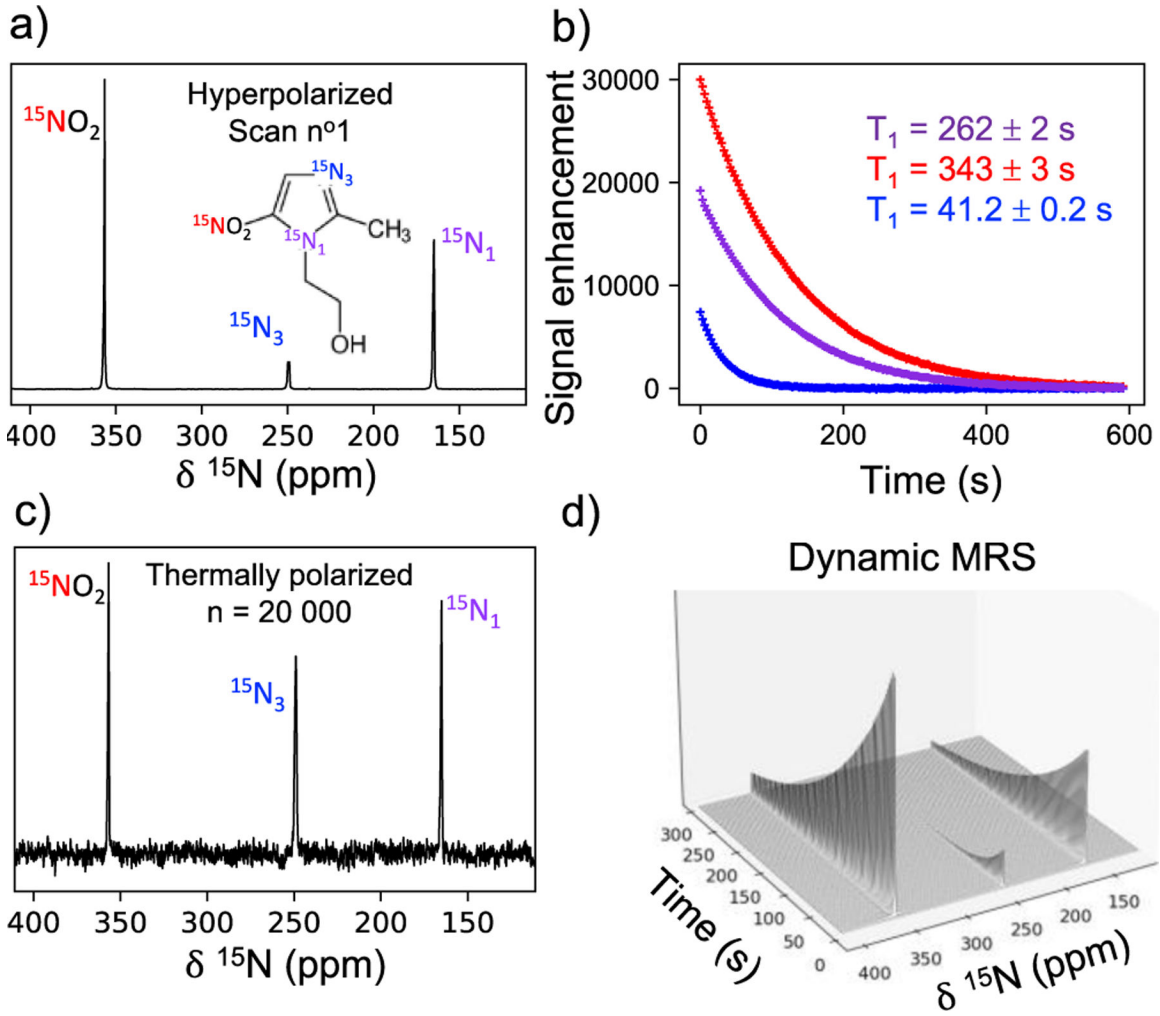


**Figure 2.**

**a)** $^{15}N$ spectrum obtained from the first scan of the HP dynamic MRS experiment. **b)** Signal enhancement as a function of time for the three [$^{15}N_3$]MNZ $^{15}N$ resonances, with color coding indicated in a). **c)** 1D spectrum at thermal equilibrium, acquired from the same sample after the HP experiment, with 20,000 averages for a total scan time of ~6 hours. **d)** Stack plot showing the signal evolution in time obtained in the HP dynamic MRS experiment.

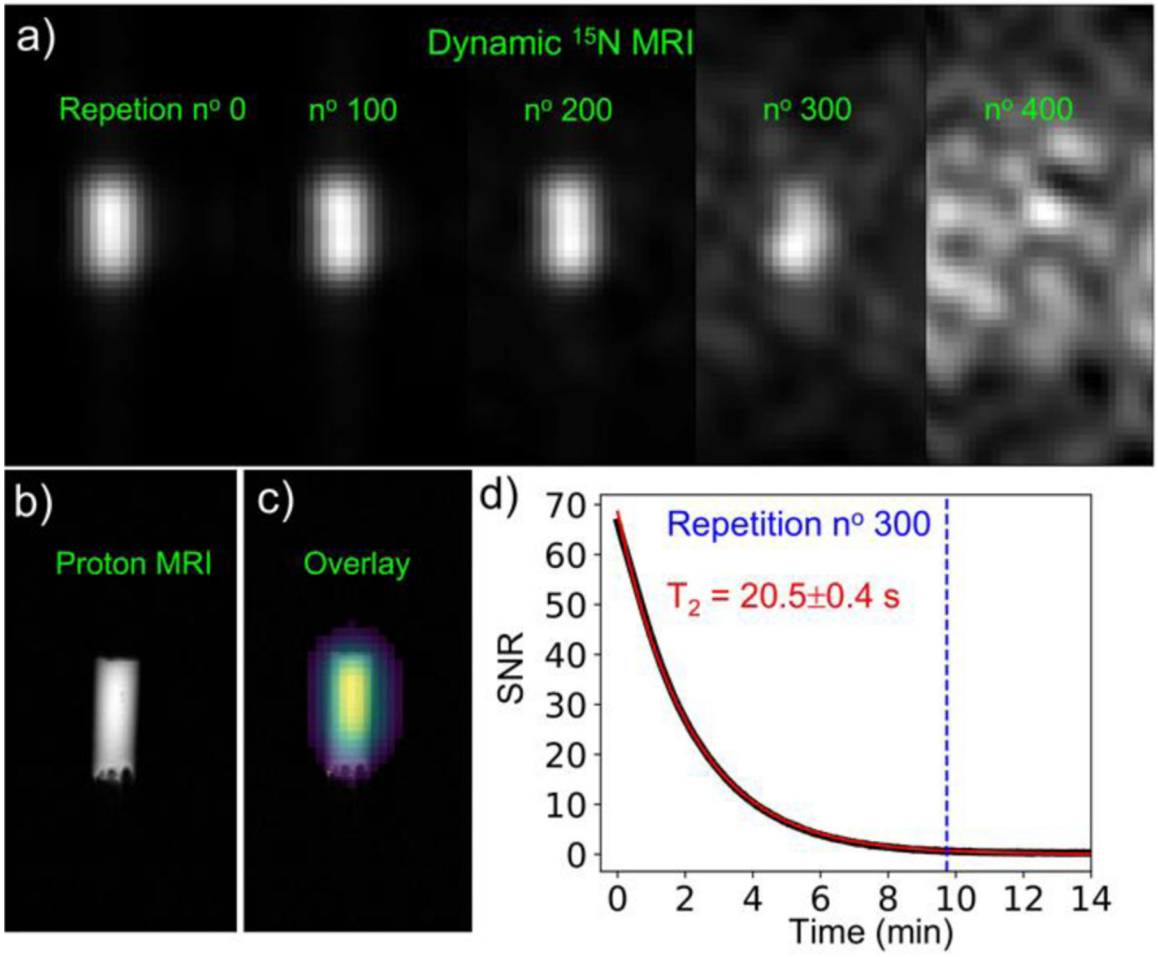


**Figure 3.**

$^{15}$N imaging of a 5-mL syringe filled with HP MNZ solution**. a)** Time series of $^{15}NO_2$ bSFFP images after 3x zero-fill, the repetition number is displayed in green. **b)** Proton image of the syringe. **c)** Overlay of the proton image and the $^{15}$N image in the first repetition of the acquisition. **d)** Long-lasting $^{15}$N HP signal measured in bSSFP acquisition. The fitted curve used to determine the $T_2$ is displayed in red. The blue dotted line represents the repetition acquired 10 min after the dissolution experiment (image shown in a, repetition nº 300).

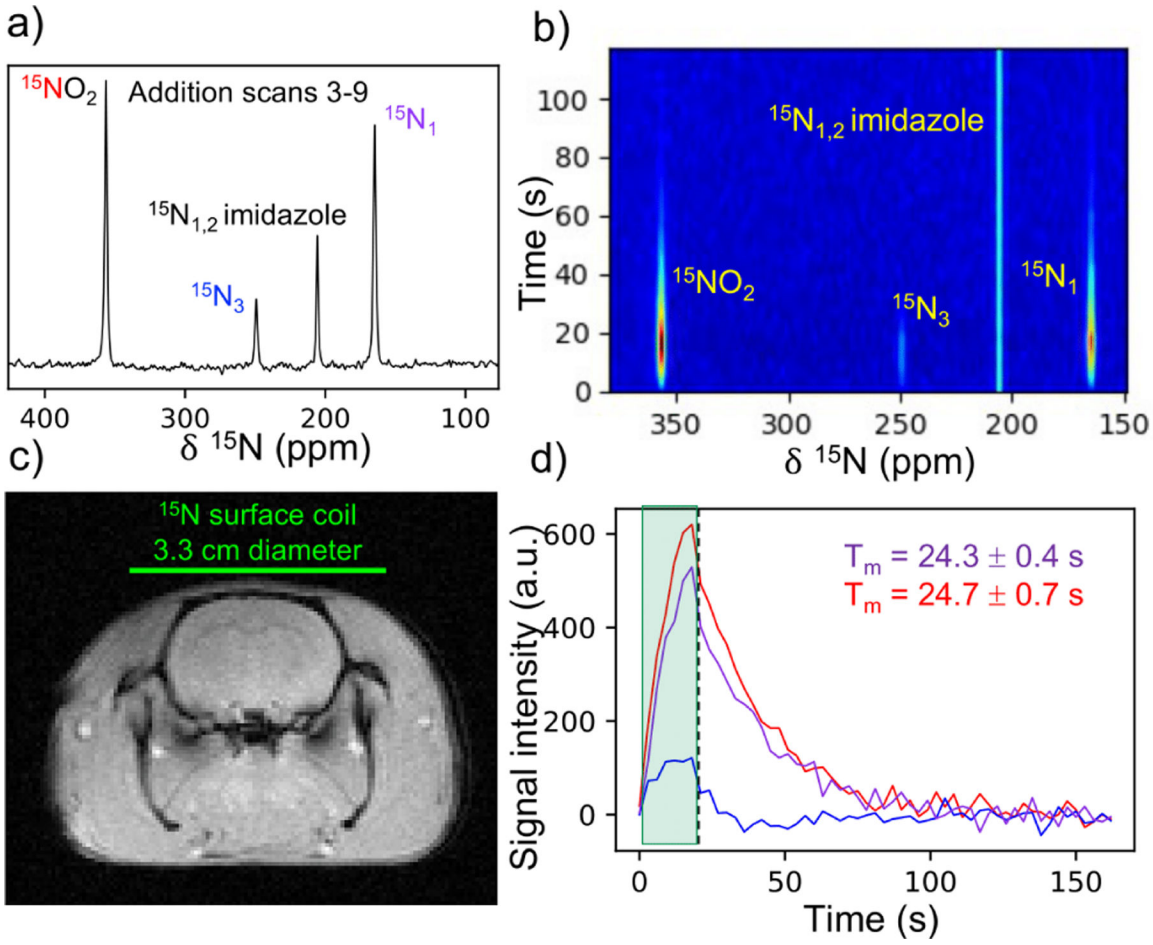


**Figure 4.**

Dynamic $^{15}$N MRS of HP [$^{15}N_3$]MNZ in rat brain with a phantom of 3M [$^{15}N_2$]imidazole on the top of the coil. **a)** Averaged spectrum of the scans 3 to 9 in the dynamic MRS series resulting in maximum SNR. **b)** Surface plot of the *in-vivo* dynamic spectroscopy experiment showing [$^{15}N_3$]MNZ signal evolution in time**. c)** Anatomical image of rat's head with the green line representing the position of the homemade $^{15}$N transmit/receive coil. **d)** Signal time curves of the three $^{15}$N sites. Colors follow the same color scheme as in a). The injection period is outlined by the green box. The Tm was extracted on the region after the black dotted line.

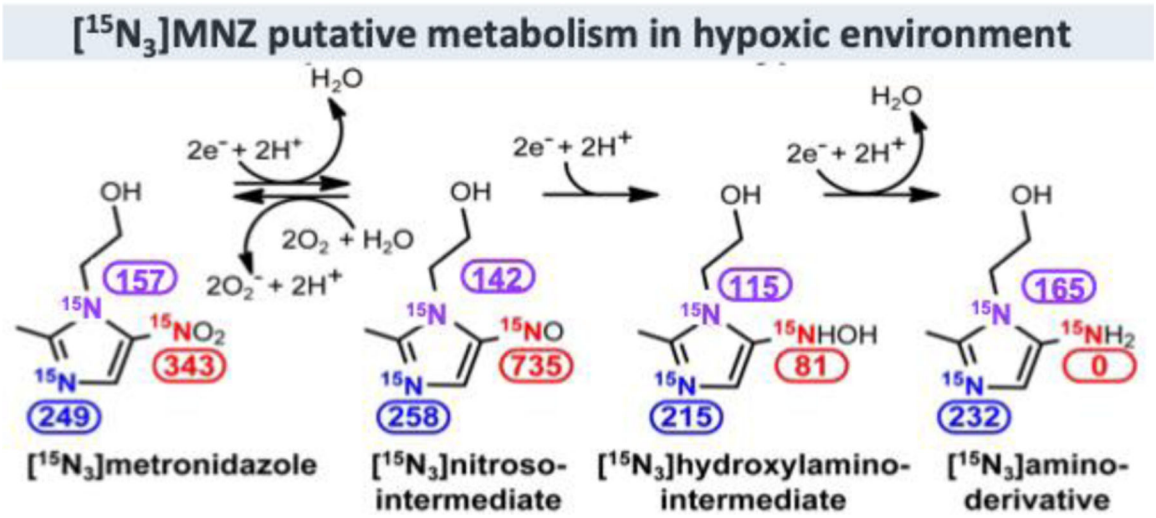


**Figure 5.**

Putative metabolism of [$^{15}N_3$]metronidazole in hypoxic biological environment[48]: the color-coded numbers denote $^{15}N$ chemical shifts of the corresponding $^{15}N$ sites.